Multiscale insights into biofilm development on hydrophobic fouling-release coatings

scientific reports

Check for updates

OPEN

Multiscale insights into biofilm development on hydrophobic fouling-release coatings

Camille Ferré[1], Laurence Gbaguidi[2], Sonja K. Fagervold[1], Claire Carrion[3], Emilie Adouane[4], Yonko Gorand[5], Lionel Nicole[2] & Raphaël Lami[1]✉

Marine biofilms develop under the combined influence of environmental conditions and substrate properties. Among antifouling strategies, fouling-release coatings (FRCs) aim to promote the detachment of microorganisms considering their surface characteristics, offering an opportunity to examine how unfavorable adhesion conditions shape microfouling processes. Hydrophobic interpenetrating polymer networks (IPNs) based on tetrafluoroethyl methacrylate (TFEMA) and a commercial PDMS-based FRC were immersed for 6 months in natural seawater (Banyuls-sur-Mer, NW Mediterranean Sea), followed by exposure to moderate hydrodynamic shear stress using a rotor device. Biofilms were analyzed through a multiscale and multiomics approach combining biomass assays, microscopy, metabarcoding, and metabolomics. Community structure varied with time and substrate, but taxonomic convergence occurred during the mature stage. Notably, fungi appeared as overlooked contributors to biofilm dynamics on low-adhesion surfaces, suggesting that their roles in FRCs warrant further attention. Exposure to moderate hydrodynamic stress induced partial biomass loss while the overall community composition was largely unaffected. Metabolomic profiles further revealed coating-specific signatures, reflecting distinct physiological strategies. Together, these findings underscore how FRC surfaces modulate biofilm maturation and resilience under mechanical stress.

Keywords Microfouling, Microbial community, Hydrophobic substrate, Fouling-release coating (FRC)

In marine environments, the colonization of submerged surfaces by organisms is both rapid and inevitable. Initial microbial adhesion is the first step in the formation of complex, multispecies biofouling communities that can persist over time[1–4]. Although this process is natural and widespread, it can lead to substantial negative ecological and economic consequences, notably by facilitating the spread of invasive species and affecting the performance, durability, and maintenance of immersed structures[2]. Numerous maritime infrastructures, including sensors, aquaculture systems, offshore platforms, and ships, are impacted[5–7]. The economic impact of marine biofouling on ship hulls, where even a thin layer of microbial slime can increase hydrodynamic drag, is particularly striking[8]. Such early-stage microfouling may raise fuel consumption by up to 40%, causing disproportionately large economic and environmental consequences through increased greenhouse gas emissions[9,10]. Biofilm-driven processes also accelerates corrosion, especially in metal-based infrastructures, compromising installation safety and longevity, and contributing to global economic losses of billions of US dollars annually[11,12].

Since these detrimental effects stem from the earliest stages of colonization, a mechanistic understanding of microbial adhesion and biofilm formation is essential to anticipate and mitigate long-term fouling development. Pioneering communities are taxonomically and metabolically diverse, comprising bacteria, archaea, microalgae, and protists, each contributing unique biochemical functions to the nascent biofilm[1]. As primary colonizers, bacteria rapidly attach to surfaces and secrete extracellular polymeric substances (EPS), forming a protective matrix that enhances survival, and facilitates the settlement of additional functional groups, thereby increasing

[1]Sorbonne Université, CNRS, UPVD, UMR8176, Laboratoire de Biodiversité et Biotechnologies Microbiennes (LBBM), Observatoire Océanologique, 66650 Banyuls-sur-Mer, France. [2]Sorbonne Université, CNRS, UMR7574, Laboratoire de chimie de la matière condensée de Paris (LCMCP), 4 Place Jussieu, 75005 Paris, France. [3]CNRS, INSERM, CHU Limoges, BISCEm, UAR 2015, US 42, Univ. Limoges, 87000 Limoges, France. [4]Department of Mechanics and Maritime Sciences, Chalmers University of Technology, 412 96 Gothenburg, Sweden. [5]Plateforme EnRMAT, Laboratoire PROMES, Rambla de la Thermodynamique, Perpignan, France. ✉email: raphael.lami@obs-banyuls.fr

biofilm complexity and persistence[13–15]. Among these functional groups, marine fungi are increasingly recognized as important contributors to biofilm structure and dynamics[16–18]. Although typically less abundant and underappreciated, marine fungi can influence biofilm stability, detachment, and overall ecological succession through matrix degradation, surface chemistry modification, and synergistic or competitive interactions with bacteria[19,20]. Their filamentous growth, metabolic versatility, and ability to produce EPS suggest that they could play key roles in shaping biofilm architecture and resilience, making them relevant targets for antifouling studies[16,21,22].

Recognizing that initial biofilm architecture governs the long-term adhesion and succession of fouling communities, fouling-release coatings (FRCs) target early microbial colonization through nontoxic surface modifications, offering an environmentally friendly alternative to traditional biocidal paints[23]. Among these, polydimethylsiloxane (PDMS) coatings are widely used for their favorable physicochemical properties, notably low surface energy and reduced elastic modulus, which facilitate organism detachment under hydrodynamic stress[23–25]. However, PDMS coatings suffer from poor mechanical durability and limited effectiveness under static or low-flow conditions[26], prompting the emergence of new materials such as organic–inorganic interpenetrating polymer networks (IPNs)[27–30]. Fluorinated compounds are typically used to reduce surface energy[31,32]. Zhang et al.[33] designed IPN coatings consisting of fluorocarbon resin/polyacrylate to lower the surface energy, thereby enhancing anti-icing and anti-fouling properties against both microbial and macrofouling organisms. While hydrophobic IPNs show strong potential, their ecological implications in marine biofouling contexts remain largely unexplored, and their efficacy depends on interactions with microbial colonizers.

In addition to their antifouling potential, FRCs also represent a valuable experimental system for studying biofilm development under unfavorable adhesion conditions. By providing surfaces with controlled physicochemical properties such as low surface energy and tailored elasticity, FRCs enable the investigation of microbial adaptation, organization, and persistence on substrates that resist colonization. While most research has focused on coating performance in marine environments, few studies have examined the taxonomic composition and dynamics of biofilm communities that develop on fouling-controlled coatings, and even fewer have specifically focused on FRCs[34–36]. Papadatou et al.[37] compared the bacterial community that developed on fouling release and biocidal coatings after four months of immersion in Langstone Harbour, UK, and confirmed differences in the biofilm profiles between coating types. Beyond initial colonization, biofilm development on engineered coatings is further shaped by hydrodynamic conditions, as shear stress strongly influences biofilm maturation, architecture, and detachment processes, thereby determining the persistence or release of mature communities[38–40]. Such environments challenge the ability of bacteria to initiate stable adhesion, shaping subsequent community assembly and biofilm architecture[41,42]. Although the ecological roles of fungi may affect biofilm succession and resilience, their contribution to the biofouling of FRCs remains poorly characterized. Understanding these dynamics is key to elucidating biofilm settlement and the ecological impacts of antifouling technologies in natural settings.

To advance this biological understanding, we investigated biofilm development on two hydrophobic fluorinated organic–inorganic IPNs and compared them with a commercial PDMS-based FRC. Materials designed to combine optimal surface energy with distinct levels of reduced elastic modulus provide a framework for examining how specific substrate properties shape biofilm maturation and stability. Surfaces were immersed in natural seawater for six months, spanning a major seasonal bloom, with biofilm formation monitored at one, three, and six months using biomass and community structure descriptors. Particular attention was given to bacterial dynamics as indicators of substrate-driven differences. Fungal communities were also analyzed to complement this perspective, offering additional insights into biofilm assembly on low-adhesion surfaces. Finally, mature biofilms on the different surfaces were exposed to controlled hydrodynamic shear stress to evaluate detachment and resilience, thereby assessing the potential of these coatings for passive biofilm release under realistic flow conditions.

Materials and methods

Coating formulation development and characterization

Two thin transparent hydrophobic organic–inorganic sol–gel materials (hereafter referred to as TFEMA–TEOS and TFEMA–DMDES) were developed to obtain surface properties tuned for marine antifouling applications[43]. Briefly, two different silicon precursors, tetraethoxysilane (TEOS) and dimethyldiethoxysilane (DMDES), were employed, while trifluoroethyl methacrylate (TFEMA) was introduced as the methacrylate monomer to confer hydrophobicity to the material. Methacryloxypropyltrimethoxysilane (MPTS) was used as a silane coupling agent. Syntheses were performed following previously established protocols[44,45]. Details of the synthesis are described in the supplementary methods. Intersleek1001 (AkzoNobel®), containing TEOS and hydroxy-terminated PDMS, served as a commercial reference. Intersleek1001 PDMS paint was prepared according to the manufacturer's instructions. Each coating was applied by liquid deposition using the dip-coating process to ensure the minimum roughness on 76 × 52 × 1 mm and 120 × 60 × 7 mm borosilicate glass slides. Uncoated glass slides were used as negative controls to compare surface properties with and without treatment[46–48]. The reduced elastic modulus (Er) was measured by nanoindentation with an Anton Paar NHT3 nanoindenter, and surface free energies were calculated according to the Owen–Wendt–Rabel–Kaelbe (OWRK) method with a Krüss DAS30 drop profile analyzer using the contact angle of Milli-Q water and diiodomethane (Table 1).

Incubation and biofilm detachment test

The slides (coated and uncoated) were incubated in 80 L aquariums with continuous unfiltered seawater pumped from the Banyuls-sur-Mer bay starting in February 2024 (Fig. S1). Temperature, pH and salinity records are available in the supplementary methods (Table S1). The flow rate was set at 5 L min^{-1}, resulting in more than three water renewals per hour. A 12-h photoperiod was ensured by artificial lighting using LED AQUAVIE Lumivie

Formulation	ER (Gpa)	γ (mN/m)
TFEMA–TEOS	4.9	26
TFEMA–DMDES	2.4	26
Commercial paint (PDMS–TEOS)	0.03	24
Uncoated substrate	70	70

Table 1. Reduced elastic modulus (Er) and surface free energy (γ) of the uncoated glass, commercial paint and TFEMA-based coatings.

RAL G2 SBM (15,000 K – 120 cm – 40 W). Samples were collected after 30, 90 and 180 days of incubation to study the biofouling settlement under static conditions. All quantitative and qualitative analyses were performed on independent sample sets, which were not shared between assays. Each slide was gently rinsed with sterile seawater to remove particles and nonadherent organisms before the biological parameters were measured. At 180 days, a subset of slides was analyzed after static incubation, while another subset was subjected to a low-intensity hydrodynamic detachment test provided by a portable rotor device[38,49,50]. The slides were attached to a drum rotated by an agitation Hei-TORQUE Core motor (Heidolph, Schwabach, Germany) and were exposed to three series of 1-minute rotations at 136 rpm, corresponding to a theoretical linear speed of 5 knots.

Surface coverage and fouling rate calculation

Post-immersion images were acquired using a Canon LiDE scanner (600 dpi, 5 replicates), and the coverage percentage was calculated through image analysis using the EBImage package in RStudio version 4.2.3[51]. Briefly, the photographs were cropped and converted to grayscale, and gray intensity thresholds were adjusted to define types of fouling[52]. The surface coverage of each rating type was estimated, and the weighted fouling rate (FRw) was determined for each sample. The classification of surface status was adapted from the biofouling categories of the U.S. Navy's Naval Ship's Technical Manual (NSTM) as proposed by Oliveira and Granhag[53]: Clean (no visible fouling), incipient slime (thin, early-stage biofilm), advanced slime (thicker, mature biofilm), and soft fouling (predominance of soft-bodied macrofoulers, and sporadic colonization by sessile invertebrates). This approach associates the observed fouling type with specific Fouling Rate (FR) categories, assigned values ranging from 0 to 100 (Table S2), which are then multiplied by the corresponding coverage percentage.

Colorimetric estimation of biofouling through crystal violet quantification

The crystal violet quantification process was based on previously established methods[54,55]. Slides (5 replicates) were dried and then immersed in a crystal violet solution (0.2% final concentration) for 15 min in the dark to allow the dye to bind to the biofilms. The samples were then carefully rinsed with water to remove any nonspecifically bound dye. Residual dye, reflecting the adherent biomass, was extracted by immersing the samples in a decolorizing solution (33% glacial acetic acid) and was thoroughly mixed prior to absorbance measurement at 540 nm (Victor® NIVO™, PerkinElmer OptiPlate). For the blanks, noncolonized samples (5 replicates) were soaked in sterile seawater and processed using the same methodology.

Chlorophyll *a* areal concentration determination

Chlorophyll *a* pigment extraction was adapted from the French standard AFNOR NF T90-117 (1999). A surface area of 28 cm^2 was scraped using a glass microfiber filter (grade GF/F, Whatman) to collect the biofilm that had developed on the slides (5 replicates). The filters were immersed in 4 mL of 90% acetone and subjected to ultrasonic treatment for 20 min, followed by a 10-min rest period at room temperature in the dark. The extract was then collected, filtered through cotton fibers to remove particles that could interfere with the absorbance measurements, and transferred directly into a 5 mL volumetric flask, which was filled with acetone and homogenized. The absorbance of the extracts was measured at wavelengths of 430, 665, and 750 nm, with a glass filter dissolved in 90% acetone used as a blank. The extracts were then acidified by adding 10 µL of 5 N hydrochloric acid directly into the cuvettes to achieve a concentration between 10^{-3} and 10^{-2} mol L^{-1}. The optical density (OD) was measured at the same wavelengths as before after 3 min of incubation. The area concentration of chlorophyll *a* was calculated using the method described by Lorenzen[56].

Confocal scanning laser microscopy (CLSM) analysis

The 3D structures of the biofilms were observed by CLSM. Biofilms were fixed in 4% paraformaldehyde solution for subsequent chlorophyll autofluorescence determination, and EPS staining. A mixture of four selected stains was prepared in sterile physiological water to target different EPS components: Concanavalin A tetramethylrhodamine conjugate (ConA-TMR, Thermofischer Scientific; 0.1 g L^{-1} final concentration) was used to stain α-polysaccharides; fluorescein isothiocyanate isomer I (FITC, Merck; 0.05 g L^{-1} final concentration) was used for proteins; 1,1′-dioctadecyl-3,3,3′,3′-tetramethylindocarbocyanine perchlorate (DiD oil, Merck; 0.08 g L^{-1} final concentration) was used for lipids; and 4′,6-diamidino-2-phenylindole dihydrochloride (DAPI, Merck; 0.0001 g L^{-1} final concentration) was used for total cells[57]. For EPS staining, samples were incubated for 30 min at room temperature in the dark and gently rinsed with sterile physiological water to remove excess stain. A replicate of each sample was kept without stain to evaluate the autofluorescence of chlorophyll.

Z-stack imaging was conducted using a ZEISS LSM880 confocal laser scanning microscope at 20× and 63× magnification[58]. For each sample, five independent Z-stacks were collected using the following excitation/emission settings: DAPI (λexc 405 nm/λem 415–490 nm), FITC (λexc 490 nm/λem 553 nm), ConA (λexc 561

nm/λem 561–642 nm), and DiD oil (λexc 641 nm/λem 644–759 nm) for EPS analysis and autofluorescence (λexc 405 nm/λem 460 nm) for chlorophyll. Three-dimensional reconstructions were generated using Imaris software (Oxford Instruments) from image stacks acquired at 20× magnification. For quantitative volumetric analyses, datasets acquired at 63× magnification were processed using the open-source software BiofilmQ[59]. Automated thresholding (Otsu algorithm) was used to segment fluorescent Z-stacks for the identification and quantification of labeled structures. Biovolumes ($\mu m^3/\mu m^2$)—i.e., the cumulative volume occupied by the fluorescent signal of interest—attributed to each specific stain were then calculated.

Extraction of total DNA and identification of colonizing communities by Illumina MiSeq-based high-throughput sequencing

Biofilm sampling and DNA extraction were conducted following previously established methods[60]. The biological material was scraped using a sterile scalpel, and the samples were subsequently rinsed with 300 µL of ultrapure water. DNA extraction was performed using the FastDNA™ SPIN Kit for Soil (M.P. Biomedicals) according to the manufacturer's protocol. Extracted DNA was quantified using a Quantus fluorometer (Promega).

DNA amplification and Illumina MiSeq sequencing were conducted by Argaly SA (Sainte-Hélène-du-LacSavoie, France; https://www.argaly.com) targeting the ribosomal small subunit 16S rRNA gene, as well as the internal transcribed spacer region (ITS1) of fungi. Bacterial primers (BACTB-F: 5′-GGATTAGATACCCTGGTAGT-3′ and BACTB R: 5′-CACGACACGAGCTGACG-3′) and primers targeting fungi (ITS5 F: 5′-GGAAGTAAAAGTCGTAACAAGG-3′ and slightly modified 5.8S_fungi: _R5′-CAAGAGATCCGTTGYTGAAAGTK-3′) were used[61–63]. DNA was amplified in three PCR replicates uniquely identified by a combination of two eight-base tags attached 5′ to the PCR primers. After amplification, all the PCR products were pooled by tag and purified using a MinElute purification kit (Qiagen GmbH). Libraries were subsequently constructed, and high-throughput sequencing was carried out by Fasteris (Geneva, Switzerland). Sequencing libraries were prepared using the Metafast protocol, and Illumina MiSeq paired-end sequencing (2 × 300 bp) of the 16S rRNA and ITS1 sequences was subsequently performed. For each primer pair, raw sequencing data were demultiplexed using the OBITools 4 obitagpcr program. All sequences were submitted to NCBI in BIOPROJECT PRJNA1336684.

The resulting FASTQ files were analyzed using QIIME2 (2025.4)[64]. Details of the analysis are described in the supplementary methods. Briefly, the barcodes and primers were removed by Cutadapt[65]. Reads were reoriented because the files were in dual-indexed-mixed orientation format. Reads were then quality-filtered, merged, denoised and chimera-checked using DADA2[66]. Representative sequence for each ASV was classified using a naïve Bayes classifier trained on the SILVA and UNITE10 databases[67,68], and sequence classification was carried out using the scikit-learn framework. The ASV tables were then exported, and the results were processed using phyloseq package[69] in RStudio version 4.2.3. A permutational multivariate analysis of variance (PERMANOVA) was performed to evaluate the influence of experimental factors (surface type, timepoints and hydrodynamic stress) on the overall variation using the vegan package[70], and principal coordinate analysis (PCoA) based on Bray–Curtis dissimilarity was performed[69].

Metabolite extraction and UHPLC-HRMS/MS analysis

The extraction process was based on previously established methods[38]. After 6 months of incubation, biofouling that developed on the different slides (5 replicates) was scraped off with a sterile scalpel and transferred to glass tubes containing 5 mL of ethyl acetate. The same procedure was followed for samples subjected to the hydrodynamic detachment test. For the blanks, noncolonized samples (5 replicates) were soaked in sterile seawater and processed using the same methodology. The mixture was then vortexed and mixed overnight at 25 °C with 110 rpm agitation. The upper organic phases were then collected in separate glass tubes, and the remaining mixture was rinsed twice with 2 mL of ethyl acetate. These organic phases were combined, and the solvent was dried using a GeneVac HT-4X vacuum centrifugal evaporator. The dried extracts were weighed and reconstituted in LC-MS grade methanol at a final concentration of 1 mg mL^{-1}.

Analyses were carried out using an Ultimate 3000 ultrahigh-performance liquid chromatography system (UHPLC, Thermo Fisher Scientific) coupled with a Q Exactive Focus Orbitrap mass spectrometer operating in high-resolution tandem MS (MS/MS FT) mode. All the samples were processed in a single randomized analytical batch with an injected volume of 3 µL of sample, following validated laboratory protocols[71]. Separation was achieved on a Luna Omega® Polar C18 column (100 × 2.1 mm, 1.6 µm; Phenomenex®, CA, USA) at 40 °C. The mobile phase consisted of 0.1% formic acid in water (A) and acetonitrile (B) at a flow rate of 0.5 mL min^{-1}. The gradient started at 5% B for 3 min before injection and during 2 min, increased linearly to 100% B at 12 min (curve 5), and was maintained for 8 min (curve 2). Ionization was performed by electrospray in positive mode (ESI^+). Full MS scans were acquired from *m/z* 100–1500 at a resolution of 70,000 with an AGC (automatic gain control) target of 10^6. Nitrogen served as the nebulizing gas (sheath: 45 psi; auxiliary: 20 psi), with a spray voltage of 3.0 kV, a capillary temperature of 320 °C, and an auxiliary gas heater of 450 °C. The S-lens RF level was 55. MS^2 scans were acquired at 17,500 resolution, with an AGC target of 10^5, an isolation window of 3 *m/z*, and stepped normalized collision energies of 20, 30, and 40%.

The LC-MS/MS data were processed using MzMine 3.4.16[60,72]. Mass detection was performed with a noise level of 5.10^6 for MS^1 and 1.10^4 for MS^2 using a centroid mass detector, and the ADAP chromatogram was constructed for a retention time between 2 and 18 min, with a minimum consecutive scan of 4, a minimum intensity of 6.10^6 and a minimum absolute height of 9.10^6[72]. The chromatograms were subsequently resolved using a local minimum resolver with an MS^1 to MS^2 precursor of 0.1 *m/z* (or 10 ppm) and a tolerance of 0.200 min for the RT filter. The chromatographic threshold was set at 85%, with a minimum search range RT/mob of 0.050, a minimum absolute height of 9.10^6, a minimum ratio of 1.70 and a minimum scan of 4. Chromatograms were deisotoped, and isotopic peaks were searched before alignment was performed (through the join aligner

algorithm): *m/z* tolerance was set at 0.001 (or 5 ppm) with a weight of 3, and RT tolerance was set at 0.200 min with a weight of 1. The blanks were ultimately removed, and gap filling was performed.

Metabolite data statistical analysis and feature-based molecular networking

The matrix of metabolites was analyzed with RStudio version 4.2.3. Data preprocessing involved sum normalization followed by autoscaling. PERMANOVA was initially performed to evaluate the influence of experimental factors (surface type and hydrodynamic stress) on overall metabolic variation using the vegan package[70]. Partial least squares discriminant analysis (PLS-DA) was subsequently applied to assess class separation and identify key discriminant metabolites with ggplot2 and mixOmics packages[73,74]. Variable importance in projection (VIP) scores derived from PLS-DA were used to evaluate the contribution of each metabolite to group differentiation[75]. Regularized Canonical Correlation Analysis (rCCA) was conducted using the mixOmics R package to identify patterns of covariation and to explore correlations between 16S rRNA gene and ITS marker datasets and metabolomic profiles[74]. The first two canonical components were retained for the analysis, and variables contributing most strongly to cross-dataset correlations were extracted based on their canonical loadings.

Featured-Based Molecular Networking (FBMN) was constructed on GNPS with a cosine of 0.7 and at least four matched fragment ions, with precursor and fragment ion mass tolerances at 0.05 Da[60,76]. Clusters with more than 10 nodes were associated with a class of compounds using GNPS (Library Search and Dereplicator) and SIRIUS 5.6.3 (molecular formula identification, ZODIAC, CSI: FingerID, and CANOPUS) annotation tools[77–82]. The annotations were added to the network using Cytoscape 3.10.0 software[83].

Results

Temporal development of microfouling on antifouling coatings

Biomass accumulation over time

Surface coverage, crystal violet staining and chlorophyll *a* quantification revealed distinct temporal and surface-dependent patterns in fouling development throughout the 6-month immersion period from February to August in the aquariums (Fig. S2; Table S3). After 30 days, incipient slime covered all the samples (FRw: 7.5 to 13.6) (Fig. S2). On the uncoated substrate and TFEMA-based coatings, the biofilms progressed to advanced stages after 90 days, with increased crystal violet retention and chlorophyll *a* accumulation. Biofilms on the commercial paint remained at early developmental stages, showing low chlorophyll *a* accumulation and decreased crystal violet retention over time.

Bacterial community dynamics

The bacterial communities were analyzed using 16S rRNA gene sequencing. Multivariate analyses using PERMANOVA (Table S4) and PCoA based on ASV-level data revealed that immersion time and surface type significantly shaped community composition (Fig. 1). Immersion time accounted for the greatest portion of the variance (R^2 = 0.278, $p < 0.001$), indicating clear temporal succession in bacterial assemblages. Nevertheless, surface type significantly influenced community structure (R^2 = 0.249, $p < 0.01$), demonstrating that biofilm composition differed according to the substrate type; notably, communities on the commercial paint remained

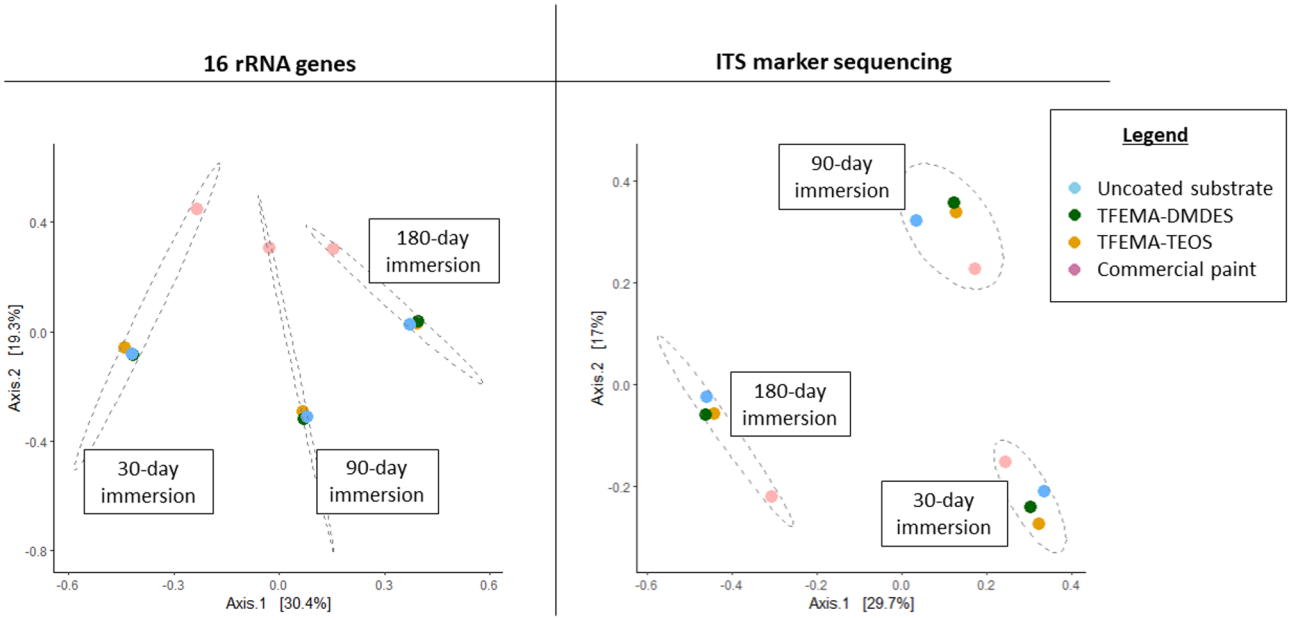

Fig. 1. Principal coordinate analysis (PCoA) of biofilm assemblages across substrate type and immersion duration based on Bray–Curtis dissimilarity of 16S rRNA gene (left) and ITS marker sequencing (right) data.

distinct, highlighting a persistent substrate effect. The interaction between immersion time and surface type was significant ($R^2 = 0.187$, $p \leq 0.005$), suggesting that colonization was modulated by the nature of the surface.

Alpha diversity indices (Chao1, Shannon, and Pielou indices) revealed temporal and substrate-dependent patterns in community richness, diversity, and evenness during immersion (Table S5). The bacterial community composition varied notably across the coatings and over time (Fig. 2). Overall, in the 16S rRNA gene dataset, between 0.2 and 10.2% of the sequences remained unassigned at the class level (Table S6); these sequences were excluded from Fig. 2, which displays only the relative abundances of the assigned bacterial classes and their nested families. Alphaproteobacteria dominated all the samples on day 30, with a relative abundance of approximately 50%, while Gammaproteobacteria were highly abundant on the commercial paint (37.3%) but less abundant on the other coatings (11.0–14.5%). After 90 days, the abundance of bacterial communities shifted significantly: Alphaproteobacteria abundance decreased to roughly 25%, while Gammaproteobacteria exhibited intermediate relative abundances (22.7–43.7%). On TFEMA–TEOS, TFEMA–DMDES and the uncoated substrate, minor taxa, including Bacteroidia, Planctomycetota, and Acidimicrobiia, increased in abundance, especially on the TFEMA–TEOS coating (24.7%, 5.3% and 9.2%, respectively). After 180 days, Alphaproteobacteria, Gammaproteobacteria and Bacteroidia tended to reach equilibrium across all samples (20–25% in average). Overall, minor taxa maintained intermediate relative abundances, with Acidimicrobiia accumulating across the three timepoints, particularly on commercial paint and TFEMA-based coatings.

Fungal community dynamics

Fungal communities were analyzed using ITS marker sequencing. The PERMANOVA (Table S7) revealed that immersion time ($R^2 = 0.272$, $p \leq 0.001$) and surface type ($R^2 = 0.222$, $p \leq 0.001$) significantly shaped community structure, with their interaction ($p \leq 0.005$) explaining 17.7% of the variance, suggesting that the temporal dynamics of colonization were modulated by surface type. Although the immersion time points formed well-separated groups on the PCoA (ASV level) (Fig. 1), the substrate effects were relatively minor, except for those of the commercial paint at 30 and 180 days.

Alpha diversity indices highlighted pronounced differences in fungal community dynamics across substrates and immersion times (Table S8). Overall, the uncoated substrate and TFEMA–TEOS supported the most stable communities. Between 6.68 and 97.63% of the fungal sequences remained unassigned at the class level (Table

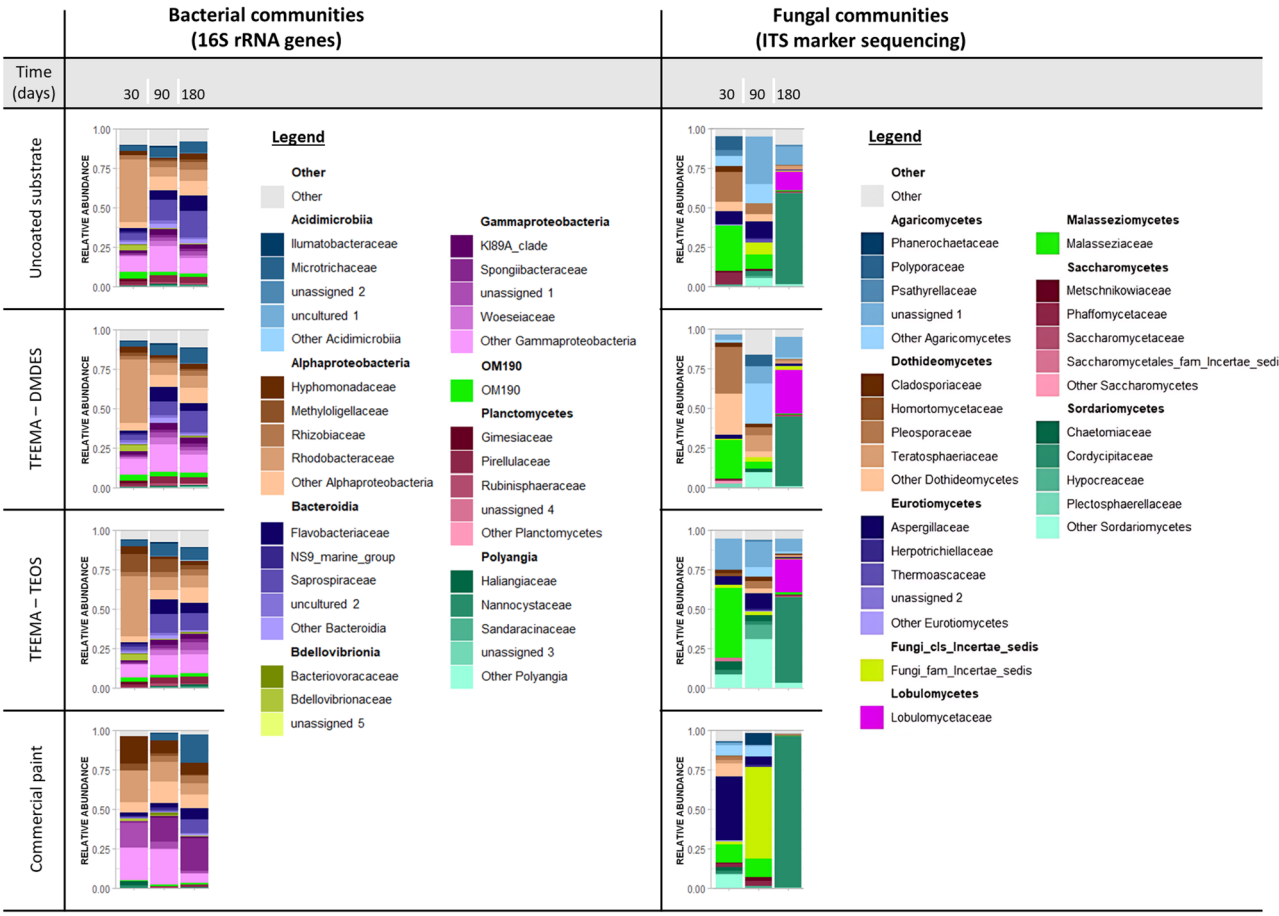

Fig. 2. Bacterial (16S rRNA gene sequencing) and fungal (ITS marker sequencing) diversity at the class and family levels across substrate types after 30, 90, and 180 days of immersion. Unassigned sequences at the class level are not shown (see Supplementary Tables S6 and S9).

S9) and are not included in Fig. 2. At 30 days, the commercial paint, TFEMA–TEOS and TFEMA–DMDES coatings were dominated by Eurotiomycetes (41.4%), Malasseziomycetes (44.3%) and Dothideomycetes (58.4%), respectively, whereas the uncoated substrate supported a more even assemblage, including Malasseziomycetes (28.8%), Dothideomycetes (28.8%) and Agaricomycetes (18.9%). Sordariomycetes became highly dominant at 90 days on the TFEMA–TEOS coating (46.2%), whereas Agaricomycetes increased on the TFEMA–DMDES coating and uncoated substrate (43.8% and 42.5%, respectively). Commercial paint was largely dominated by unassigned fungal classes (58.3%). A marked convergence toward fewer dominant taxa was further observed, with a strong dominance of Sordariomycetes, especially on commercial paint (96.6%). Notably, Malasseziomycetes, Eurotiomycetes and Dothideomycetes, which were prevalent during early colonization, nearly disappeared by this stage (< 5% on all surfaces).

Microfouling resilience and restructuring under low-adhesion conditions combined with hydrodynamic shear stress

Biofilm detachment

After 180 days of immersion in the aquariums, the different surfaces were exposed to a 5-knot hydrodynamic shear stress to evaluate the detachment and resilience of mature biofilms, thereby assessing the potential of these coatings for passive biofilm release under flow conditions. Surface coverage assessment was performed to evaluate the effect of 5-knot hydrodynamic shear stress on fouling across substrates (Fig. S3; Table S10). Across all the surfaces, hydrodynamic stress generally caused partial biofilm detachment, reducing the thickness and complexity of the microfouling, consistent with decreased FRw indices as well as with crystal violet and chlorophyll *a* quantification (Fig. S4). Confocal microscopy revealed that the biofilms were largely dominated by polysaccharides across all surfaces after six months of incubation, while notable differences in lipid and protein proportions were observed depending on the coating type and following hydrodynamic stress (Fig. S5).

Microbial community structure

The microbial community was characterized before and after shear stress. Multivariate analysis of community composition using PERMANOVA revealed significant effects of both hydrodynamic conditions and coating type on biofilm assemblages (Table S11). Coating type explained the greatest percentage of the variation ($R^2 = 0.365$, $p = 0.001$), indicating strong surface-dependent structuring of the bacterial communities. A PCoA highlighted these differences in the composition of the different sample groups, revealing a high degree of similarity between the TFEMA-based coatings and the uncoated substrate (Fig. 3; Table S12). Hydrodynamic conditions also influenced the biofilm composition but to a lesser extent than the substrate type did ($R^2 = 0.047$, $p = 0.001$). The TFEMA–DMDES coating showed the greatest variation (Fig. 3). In addition, a significant interaction between condition and coating type ($R^2 = 0.079$, $p = 0.024$) highlighted that the impact of hydrodynamic stress on microbial community assembly differed depending on the underlying surface.

Before the application of hydrodynamic stress, the alpha diversity indices indicated strong variability: marked differences in community structure were evident among the coatings, with the TFEMA-based materials and uncoated substrate generally supporting richer and more diverse assemblages than the commercial paint did (Table S13). After 180 days of static incubation, the bacterial assemblages on the different coatings consisted

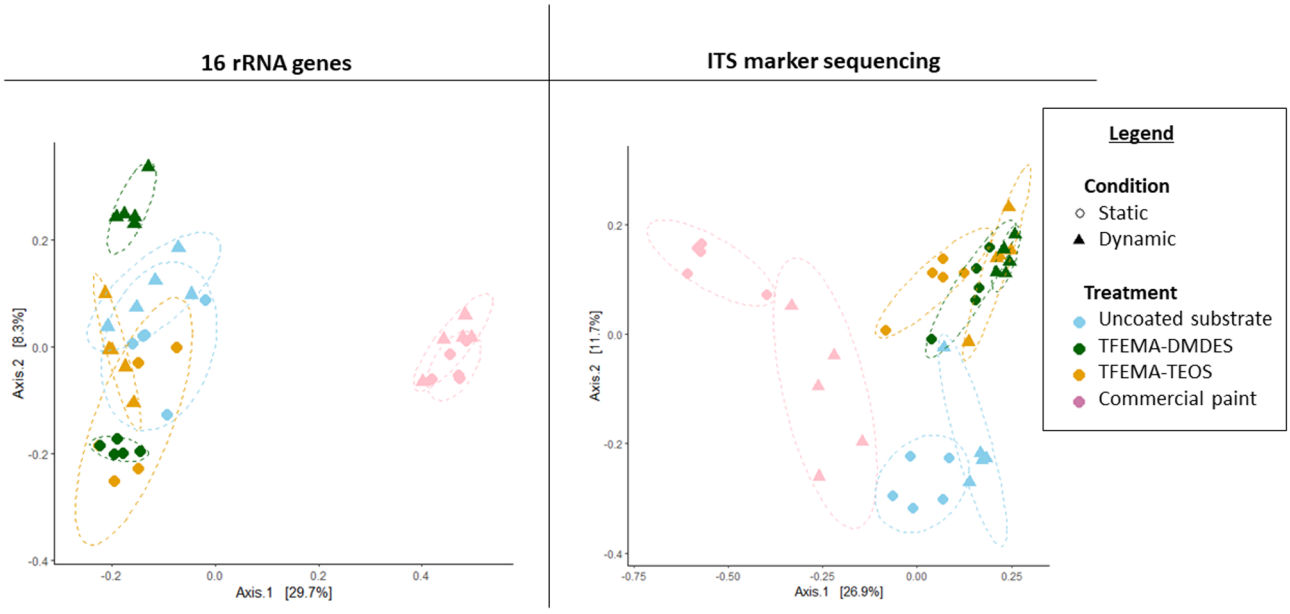

Fig. 3. Principal coordinate analysis (PCoA) of biofilm assemblages across substrate type and hydrodynamic shear stress on the basis of the Bray–Curtis dissimilarity of 16S rRNA gene (left) and ITS marker sequencing (right) data.

of Alphaproteobacteria, Gammaproteobacteria, and Bacteroidia, with some contribution from Acidimicrobiia and other minor taxa (Fig. 4). Following hydrodynamic stress, however, the relative abundances of several bacterial classes changed across substrates. In particular, Gammaproteobacteria became the dominant class in the commercial paint (34.8%). On the TFEMA–TEOS coating, the distribution became more balanced, with minor taxa such as Acidimicrobiia (9.3%) and Planctomycetota (5.7%) showing increased relative abundances. Overall, Bacteroidia appeared less impacted by hydrodynamic stress across all surfaces and rose to dominance on the TFEMA–DMDES coating and uncoated substrate, while secondary taxa (such as Planctomycetota) were enriched.

PERMANOVA was performed to assess the effects of hydrodynamic condition, coating type, and their interaction on fungal community composition (Table S14). Both factors had significant effects on community structure (condition: $R^2 = 0.062$, $p = 0.001$; treatment: $R^2 = 0.291$, $p = 0.001$). The PCoA results revealed a strong similarity between the two TFEMA-based coatings, both before and after shear stress, whereas the uncoated substrate and the commercial paint formed two distinct groups before shear stress (Fig. 3). After the hydrodynamic stress, the groups tended to converge. Importantly, the interaction between condition and coating type was also significant ($R^2 = 0.108$, $p = 0.001$), indicating that the response of fungal communities to hydrodynamic stress depended on the surface type.

The alpha diversity indices revealed that hydrodynamic conditions altered fungal community diversity depending on the surface (Table S15). After 180 days of immersion, the fungal communities at the class level consistently differed before and after hydrodynamic stress across all the coatings (Fig. 4). Between 6.68 and 97.60% of the fungal sequences remained unassigned at the class level (Table S16) and are not included in Fig. 4. On static surfaces, Sordariomycetes were generally dominant, ranging from 44.7% on the TFEMA–DMDES coating to 96.6% on the commercial paint. However, when the coatings were exposed to hydrodynamic stress, the composition shifted toward greater diversity and redistribution among classes. Overall, the abundance of Sordariomycetes decreased markedly, whereas that of minor taxa increased. While the uncoated substrate, commercial and TFEMA–TEOS coatings were further characterized by a dominant taxa (Agaricomycetes, Sordariomycetes, and Lobulomycetes, respectively), the TFEMA–DMDES coating resulted in a more even community distribution with Sordariomycetes (30.4%), Agaricomycetes (28.3%), and Lobulomycetes (23.1%).

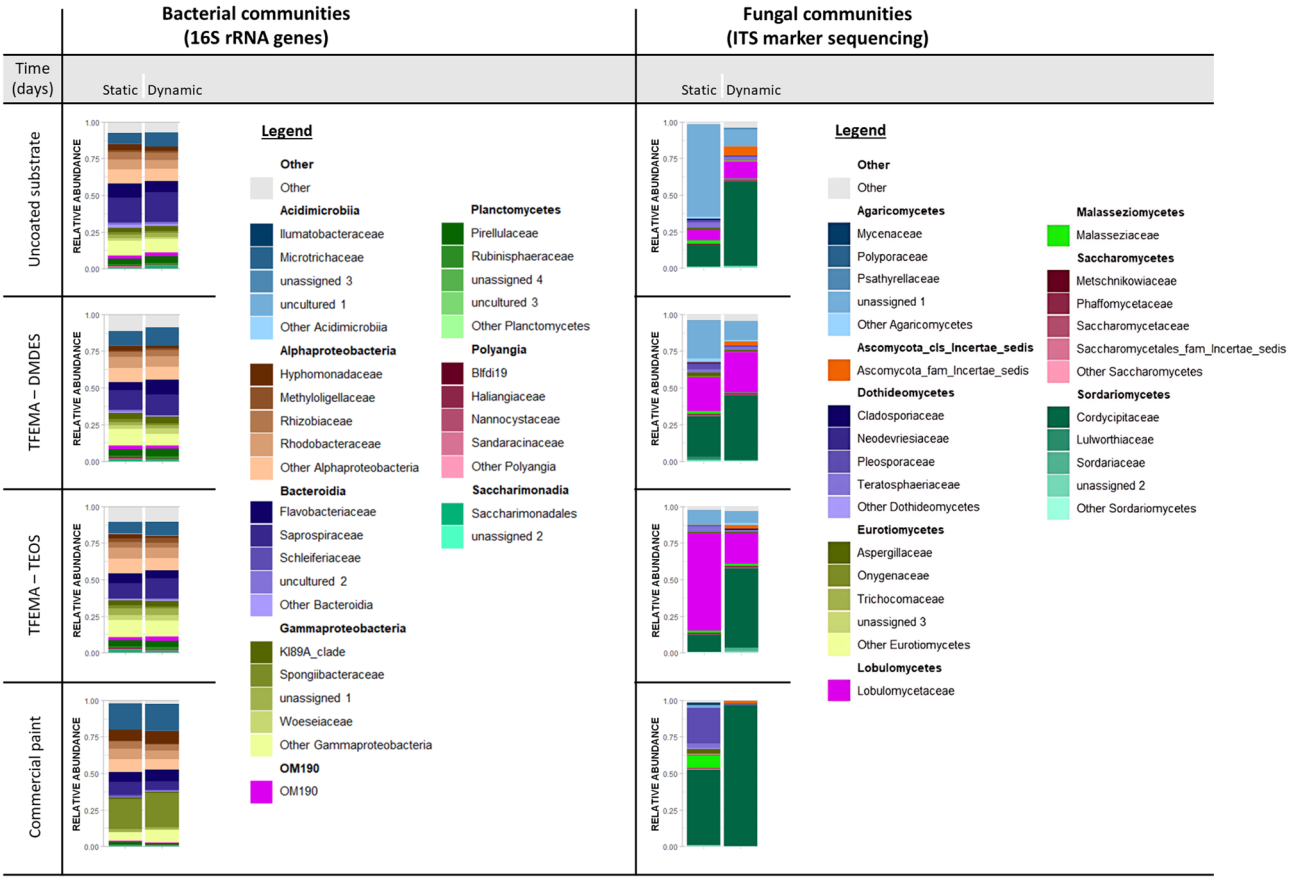

Fig. 4. Bacterial (16S rRNA gene sequencing) and fungal (ITS marker sequencing) diversity at the class and family levels across substrate types before and after 5-knot hydrodynamic shear stress. Unassigned sequences at the class level are not shown (see Supplementary Tables S12 and S16).

Metabolite diversity and integrated microbial–metabolomic response to low-adhesion conditions combined with hydrodynamic shear stress

Untargeted metabolomics analysis was conducted to compare the variations in metabolites before and after 5-knot hydrodynamic shear stress. PERMANOVA revealed a significant effect of surface type on metabolite composition ($R^2 = 0.328$, $p \leq 0.001$), indicating that each biofouling community has a distinct chemical signature depending on the surface (Table S17). In contrast, the effect of low hydrodynamic stress alone was modest and not statistically significant ($R^2 = 0.0237$, $p = 0.188$), suggesting that the applied stress did not induce major shifts in the metabolomic landscape. However, the interaction between the surface type and the hydrodynamic stress contributed significantly ($R = 0.13.8$, $p = 0.015$), revealing that the changes in the metabolome after the stress varied depending on the surface considered. PLS-DA revealed distinct clustering of the metabolomic profiles according to substrate (Fig. 5, Table S18). Within each substrate group, the static and dynamic groups tended to overlap, suggesting that compared with substrate-driven differences, hydrodynamic shear had only a limited effect on the overall metabolic signature.

The molecular network generated with GNPS provided a structured overview of the metabolomic profiles, highlighting both shared and substrate-specific features (Fig. 6, Fig. S6), and showed the *m/z* features that best contributed to the separation between the different surfaces, according to their VIP scores extracted from the PLS-DA model (Fig. S7). Among the 1,215 *m/z* features, 462 were detected across all sample types, reflecting a common core metabolome associated with biofilm communities, including large clusters of monogalactosyldiacylglycerols (MGDG), diagalactosyldiacylglycerols (DGDG), mono-, di- and tri-acylglycerols, and phenylethylamines. Carotenoids and chlorophyll-related compounds were also found in all the samples, with a predominance on the uncoated substrate and TFEMA-based coatings, in accordance with the quantification of the amount of chlorophyll *a* (Fig. S4). In contrast, distinct clusters of features were associated with commercial paint versus TFEMA-based coatings and the uncoated substrate, confirming that surface properties strongly modulated the biochemical landscape. Specifically, 114 *m/z* features were associated only with the commercial paint, among which several were linked with ceramides and glycerolipid clusters (I, K, O). Two VIP metabolites were grouped within the fatty amide cluster (N), which was predominantly linked to commercial paint biofilms. The DMDES-based coating distinguished itself by 88 unique *m/z* features distributed mainly across glucosinolate and tripeptide clusters (P, H), with the tripeptide cluster comprising five VIPs, and was also overrepresented in a large unannotated cluster. No specific metabolite cluster was associated with compound categories affected by shear stress; however, 167 *m/z* features disappeared after exposure, whereas 55 new features emerged, essentially on uncoated substrates and TFEMA-based coatings.

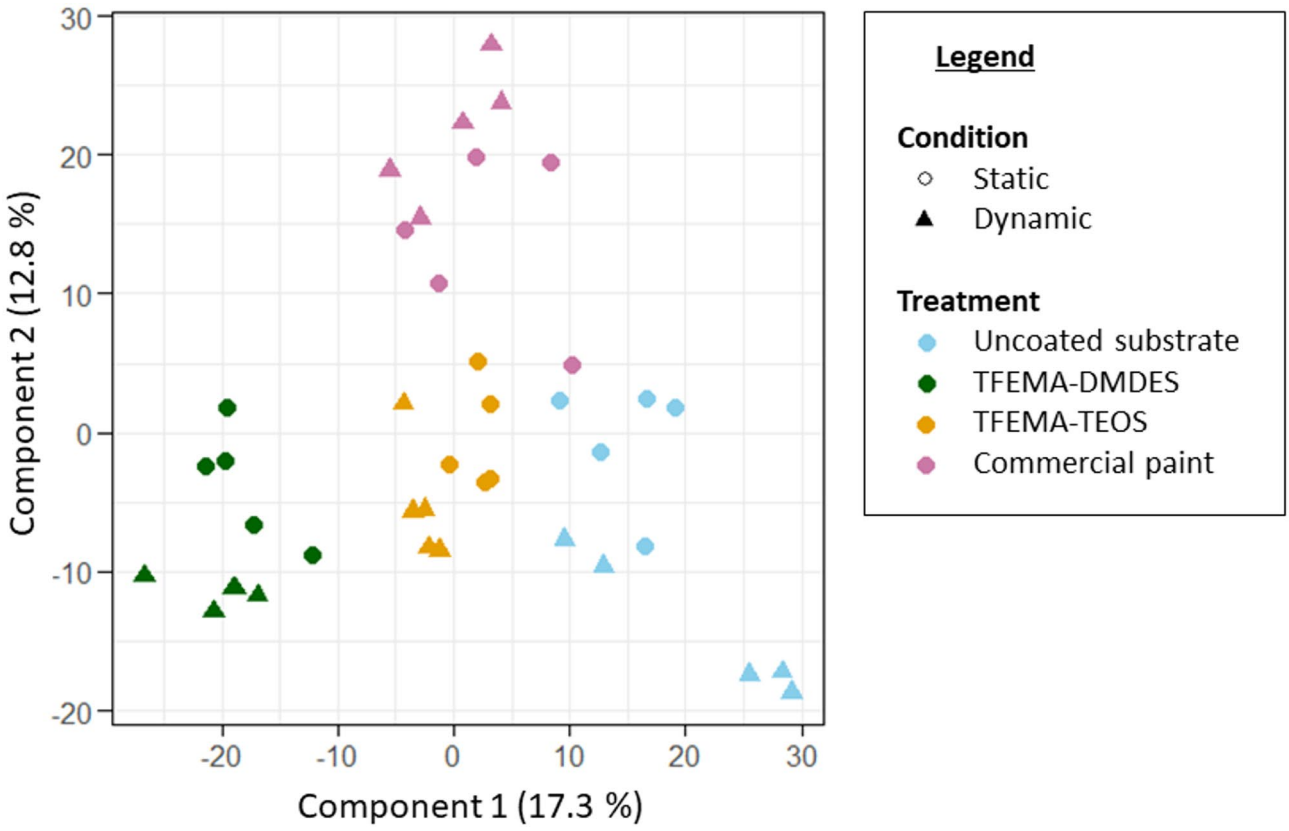

Fig. 5. PLS-DA score plot illustrating substrate-driven clustering of biofilm metabolomic profiles under hydrodynamic shear stress.

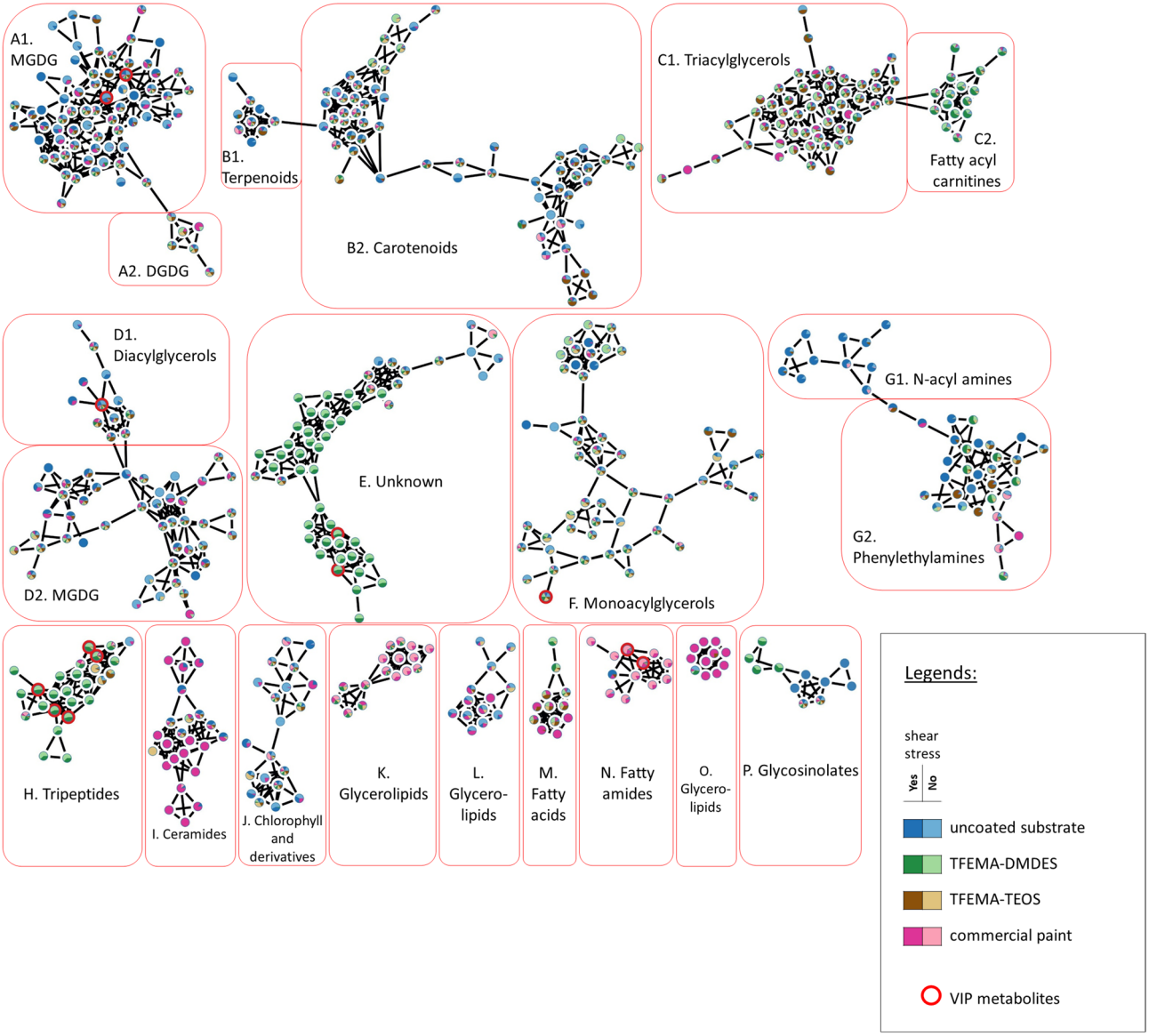

Fig. 6. Putative metabolites extracted from biofilms grown on uncoated substrate, TFEMA–TEOS, TFEMA–DMDES and commercial paint during a 6-month incubation in natural seawater before and after 5-knot hydrodynamic shear stress. Featured-Based Molecular Networking generated on GNPS with parameters Min Pairs Cos = 0.7 and Min Matched Fragment Ions = 4. The node color chart represents the proportion of each substrate type (with and without hydrodynamic shear stress) for the considered ions on the basis of peak area. Only clusters with more than 10 compounds are shown and were annotated after their pathway, superclass or class using Sirius 5.6.3. automatic annotation (molecular formula identification, ZODIAC, CSI: FingerID and CANOPUS) coupled to manual putative annotation using Thermo Freestyle.

To investigate the relationship between microbial communities and metabolomic profiles, rCCA was applied to 16S rRNA gene and ITS marker datasets. Bacterial ASVs exhibited structured, taxon-specific correlations with metabolomic features, indicating coordinated and functionally relevant responses across substrates (Fig. S8). Notably, two Gammaproteobacteria (Alteromonadaceae and Marinomonadaceae) were negatively correlated with VIP features X413 and X416 (Fig. S7, Table S19). In contrast, fungal ASVs showed a global covariation with the metabolome, driven by a single canonical component, with limited dispersion and strong taxon-metabolite specificity. Seven bacterial ASVs were correlated to ten metabolites, whereas only one fungal ASV showed a strong negative correlation. Interestingly, the feature X382 putatively identified as a lyso-MGDG C20:5 was negatively correlated with Alteromonadaceae and Marinomonadaceae and the Tremellomycetes *Vishniacozyma victoriae*.

Discussion

This study aimed to evaluate the development and resilience of biofilms on two fluorinated organic–inorganic IPN coatings, a commercial PDMS-based fouling-release reference and an uncoated substrate. All experiments were conducted at the laboratory mesocosm scale in aquariums continuously supplied with natural unfiltered seawater pumped in the bay of Banyuls-sur-Mer, providing controlled yet environmentally relevant conditions. By combining temporal analyses of biomass and community composition with hydrodynamic stress experiments, we provided insights into both the colonization dynamics and the detachment potential of mature biofilms under flow conditions.

Biofilm development followed a consistent growth pattern influenced by both natural succession processes and substrate type. All the samples were rapidly colonized by microfouling, despite the physicochemical properties of the materials being optimized according to Baier's criteria[84]. Overall, the TFEMA-based coatings supported biofilm levels similar to those of the uncoated substrate, whereas the commercial coating maintained lower biomass accumulation and limited biofilm progression after initial colonization. However, the accumulation of biofilm on glass remained limited, reflecting its physicochemical properties that inherently restrict organism adhesion[85].

These temporal shifts underscore the predominant role of environmental drivers on biofilm accumulation, often outweighing substrate-specific effects, which is consistent with studies showing that surface properties are secondary to environmental pressures in shaping biofilm dynamics[13,34,36,86,87]. Overall, uncoated substrates and TFEMA-based coatings progressed toward advanced slime stages, whereas commercial paint mainly affected early colonization. As the biofilms matured, the microbial community structure converged across the surfaces, in line with the homogenization reported in older communities[88]. After 180 days of immersion, polysaccharides were predominant across all surfaces, reflecting their key role in structural stability[15,89]. Nevertheless, TFEMA-based coatings were distinguished by their lipid and protein proportions, highlighting the influence of surface properties on biofilm physiochemistry and architecture, which is consistent with recent reviews on matrixome adaptability to physicochemical cues[90]. Metabolomic analyses further revealed MGDG, DGDG, and acylglycerols in the mature biofilm as part of the core metabolome, in agreement with previous findings describing these lipid families as classical membrane components, energy reserves and secondary metabolites of marine microorganisms[38,91]. Interestingly, some metabolite classes were specific to certain coatings, suggesting the presence of coating-dependent metabolic fingerprints. Ceramides, which were particularly represented in commercial paint biofilms, are increasingly recognized as biofilm-associated signaling adaptation molecules whose accumulation may indicate physiological adjustments within the microbial assemblage[92]. Along with ceramides, biofilms on the commercial paint were enriched in glycerolipids and fatty amides, consistent with the CLSM observations suggesting a lipid-rich matrix that may enhance adhesion to the hydrophobic substrate. In contrast, the high abundance of peptides and glucosinolates in TFEMA-associated biofilms could confer distinct flexibility potentially modulating cell–cell interactions and signaling, and enhancing the adaptative response of the biofilm to environmental fluctuations[93–95]. Moreover, the multi-omics analyses suggested that bacteria directly influenced specific metabolite profiles, whereas fungi contributed to a general metabolic state, highlighting fundamentally different modes of functional coupling between bacterial and fungal communities with the metabolome.

Biofilm maturation was accompanied by a gradual increase in bacterial richness, reflecting sequential microbial recruitment. Zhang et al.[64] reported that core microbial groups persist across diverse substrates and broad spatio-temporal scales, while maintaining essential functional traits such as matrix formation, environmental stress response, which are ubiquitous in several bacterial groups. Consistent with this, Alphaproteobacteria dominated early colonization, but their relative abundance decreased over time. In contrast, the abundance of Bacteroidia increased on TFEMA-based coatings and the uncoated substrate, contributing to mature biofilms, whereas Gammaproteobacteria exhibited coating-dependent dynamics, dominating the commercial paint after 90 days of immersion but declining thereafter. However, the richness of the commercial paint remained relatively low, suggesting reduced successional turnover. The influence of substrate properties on biofilm diversity and function remains unclear, largely because of the limited number of studies employing high-resolution approaches that jointly assess community structure[96]. Minor taxa such as Acidimicrobiia and Planctomycetota accumulated over time on most surfaces, suggesting that early colonizers set the stage for the recruitment of less abundant, but functionally relevant taxa and that coating composition strongly influences both the temporal succession and community structure of marine biofilms.

Fungal communities, often overlooked in marine biofouling research, may critically shape biofilm structure and function on antifouling coatings. In this study, substrate properties strongly influenced fungal succession: Uncoated substrate and TFEMA–TEOS coating supported stable, balanced assemblages, whereas TFEMA–DMDES favored simplified communities. Notably, commercial paint displayed a U-shaped temporal pattern, which was also evident in macroscopic and crystal violet observations. These findings highlighted time-driven ecological assembly as a primary driver of marine fungal communities, with surface material playing a secondary role, in contrast with previous studies on plastic that reported little differentiation among materials[97–99]. Changes in alpha diversity reflected typical successional patterns reported for marine fungi, where initial richness gives way to competitive exclusion and functional specialization as biofilms mature[97,98]. Shifts in community composition, such as early surface-dependent dominance by Malasseziomycetes, Dothideomycetes, and Eurotiomycetes, followed by bloom-driven transitions to Sordariomycetes, Saccharomycetes, and enrichment in Lobulomycetes, mirror documented ecological successions in aquatic fungal assemblages[100]. Sordariomycetes, which emerged as the dominant class after 180 days of immersion in all the samples, belongs to the Ascomycota phylum, which has likewise been reported in the literature as the most abundant group within aquatic fungal communities[101–103]. However, high proportion of unassigned fungal ASVs highlights persistent challenges in marine fungal taxonomy, given inadequate database representation and frequent inability to resolve taxa beyond

class or phylum level, which impact the interpretation of diversity, succession, and ecological function in biofilm studies[20,104–106].

Nevertheless, in addition to their contribution as primary colonizers or secondary settlers, fungi produce EPS that increase matrix cohesion and mechanical stability[107,108]. Their metabolic versatility enables the degradation of complex organic compounds, thereby promoting nutrient cycling and facilitating bacterial colonization and succession[20]. Furthermore, Kjeldgaard et al.[109] suggested that fungal hyphae can act as physical scaffolds within terrestrial biofilms, increasing structural heterogeneity and providing niches for bacterial interactions, competition, and cooperation. Such functional attributes suggest that fungi may significantly shape community assembly on low-adhesion surfaces, yet their ecological roles remain largely underexplored in the context of FRCs. Integrating fungal diversity and activity into antifouling assessments is therefore essential to better understand biofilm dynamics and identify overlooked biological processes influencing the long-term performance of novel coatings. Beyond strictly FRCs, investigations of fungal communities in an antifouling context may be particularly relevant, as marine fungi can mobilize metals, act as biosorbents for various elements (including Fe, Mn, Hg, Ni, Zn, Ag, Cu, Cd, Pb), and degrade synthetic pollutants such as pesticides, mitigating their toxicity[110–113].

Hydrodynamic forces are key drivers of biofilm dynamics in natural environments since they can promote the removal of weakly attached cells[38,114,115]. FRCs are typically considered effective only at high velocities (> 10 knots), where the shear stress exceeds the adhesive strength of biofoulants[23]. However, we showed that even moderate shear stress (5 knots), comparable to conditions occurring in coastal waters (where the biofouling pressure is the highest) or during slow vessel motion, can trigger measurable biofilm detachment from FRCs, depending on the coating chemistry. These findings align with previous microfluidic experiments demonstrating that moderate laminar flows can dislodge microbial cells from thin biofilms in a thickness-dependent manner, where structural heterogeneity and flow paths may explain greater detachment from more colonized materials[115].

In addition to biomass loss, hydrodynamic shear stress affected community organization, with distinct substrate-dependent responses. The TFEMA–DMDES coating resulted in effective biofilm removal, whereas commercial paint consistently supported sparse and uneven assemblages, regardless of shear stress. Metabolomic fingerprints revealed substrate-driven clustering, indicating that compared with hydrodynamic stress, surface properties exerted a stronger influence on community physiology. Most metabolites remained relatively stable before and after hydrodynamic stress, although a subset displayed stress-dependent shifts, suggesting subtle metabolic adjustments to certain substrates. Similar observations were reported by Portas et al.[39], who highlighted the effects of shear stress on community dynamics and revealed specific patterns depending on the degree of hydrodynamic stress. Moreover, only minor changes in biofilm compositional structure were observed after hydrodynamic stress, most notably on the TFEMA-based coatings. The enrichment of secondary taxa suggested that mechanical disturbance reshaped the dominant groups while increasing the ecological contribution of less abundant lineages. Fungal communities were particularly responsive, showing systematic reductions in Sordariomycetes dominance and concomitant increases in alternative classes from Chytridiomycota depending on the substrate. This trend indicated that hydrodynamic shear stress exerted substrate-specific selective filtering on fungal assemblages, potentially by dislodging large propagules or disrupting hyphal structures, thereby creating ecological opportunities for secondary colonizers[109]. While biomass removal occurred on all the substrates, community restructuring varied with surface properties and resident taxa, highlighting the need to account for hydrodynamic variability in antifouling assessments, as even moderate flows can alter the persistence and organization of microfouling communities.

While hydrophobicity is an important property for FRCs, biofouling resistance also depends on factors such as surface chemistry, topography, roughness, incorporation of hydrophilic or amphiphilic components, and the capacity to maintain surface hydration[23,40]. Nevertheless, hydrophobic and superhydrophobic coatings remain relevant antifouling approaches, as their water-repellent properties can be combined with anti-icing and anticorrosion functions to provide durable protection for submerged structures[33,116]. Beyond biofilm development, these results raise broader considerations for antifouling strategies, with PDMS-based elastomers standing out as the benchmark FRC material and being the most extensively studied[23]. Nevertheless, fluorinated polymers have attracted attention in the marine coating field, and despite environmental concerns over PFAS and increasing pressure to limit their use, fully replacing their hydrophobic properties and chemical stability remains challenging[117]. Ongoing research on fluorinated hydrophobic coatings aims to improve their performance and develop more sustainable formulations. From a biological perspective, assessing their surface properties directly influences microbial adhesion. Thus, understanding biofouling on these polymers provides insights into the persistence and limitations of hydrophobic coatings while placing them in the broader framework of FRC technologies and supporting innovation in marine coatings.

Data availability

The datasets generated in this study are available from the corresponding author upon reasonable request. All metabarcoding sequences have been submitted to NCBI under the BIOPROJECT PRJNA1336684.

Received: 27 October 2025; Accepted: 7 January 2026
Published online: 03 February 2026

References

1. Dang, H. & Lovell, C. R. Microbial surface colonization and biofilm development in marine environments. *Microbiol. Mol. Biol. Rev.* **80**, 91–138 (2015).
2. Dobretsov, S. & Rittschof, D. Love at first taste: induction of larval settlement by marine microbes. *Int. J. Mol. Sci. 2020*. **21**, 731 (2020).

3. Qian, P. Y., Lau, S. C. K., Dahms, H. U., Dobretsov, S. & Harder, T. Marine biofilms as mediators of colonization by marine macroorganisms: implications for antifouling and aquaculture. *Mar. Biotechnol.* **9**, 399–410 (2007).
4. Zardus, J. D., Nedved, B. T., Huang, Y., Tran, C. & Hadfield, M. G. Microbial biofilms facilitate adhesion in biofouling invertebrates. **214**, 91–98. https://doi.org/10.2307/25066663 (2008).
5. Delauney, L., Compare, C. & Lehaitre, M. Biofouling protection for marine environmental sensors. *Ocean Sci.* **6**, 503–511 (2010).
6. Fitridge, I., Dempster, T., Guenther, J. & de Nys, R. The impact and control of biofouling in marine aquaculture: a review. *Biofouling* **28**, 649–669 (2012).
7. Hopkins, G. et al. Managing biofouling on submerged static artificial structures in the marine environment—assessment of current and emerging approaches. *Front. Mar. Sci.* **8**, 759194 (2021).
8. Schultz, M. P. Effects of coating roughness and biofouling on ship resistance and powering. *Biofouling* **23**, 331–341 (2007).
9. Farkas, A., Song, S., Degiuli, N., Martić, I. & Demirel, Y. K. Impact of biofilm on the ship propulsion characteristics and the speed reduction. *Ocean Eng.* **199**, 107033 (2020).
10. Schultz, M. P., Bendick, J. A., Holm, E. R. & Hertel, W. M. Economic impact of biofouling on a naval surface ship. *Biofouling* **27**, 87–98 (2011).
11. Skovhus, T. L., Eckert, R. B. & Rodrigues, E. Management and control of microbiologically influenced corrosion (MIC) in the oil and gas industry—Overview and a North sea case study. *J. Biotechnol.* **256**, 31–45 (2017).
12. Tuck, B., Watkin, E., Somers, A. & L Machuca, L. A critical review of marine biofilms on metallic materials. *NPJ Mater. Degrad.* **6** (1), 6–25 (2022).
13. Salta, M., Wharton, J. A., Blache, Y., Stokes, K. R. & Briand, J. F. Marine biofilms on artificial surfaces: structure and dynamics. *Environ. Microbiol.* **15**, 2879–2893 (2013).
14. Flemming, H. C. et al. Biofilms: an emergent form of bacterial life. *Nat. Rev. Microbiol.* **14**, 563–575 (2016).
15. Flemming, H. C. & Wingender, J. The biofilm matrix. *Nat. Rev. Microbiol.* **8**, 623–633 (2010).
16. Adouane, E. et al. Importance of quorum sensing crosstalk in the brown Alga Saccharina latissima epimicrobiome. *iScience* **27**, 109176 (2024).
17. Velázquez, D. et al. Ecosystem function decays by fungal outbreaks in Antarctic microbial Mats. *Sci. Rep.* **6** (1), 6–22954 (2016). (2016).
18. Yu, S., Lu, X. & Lu, H. Marine microbial biofilms on diverse abiotic surfaces. *Front. Mar. Sci.* **12**, 1482946 (2025).
19. Amend, A. et al. Fungi in the marine environment: open questions and unsolved problems. *mBio* **10**, (2019).
20. Zeghal, E., Vaksmaa, A., Vielfaure, H., Boekhout, T. & Niemann, H. The potential role of marine fungi in plastic degradation—a review. *Front. Mar. Sci.* **8**, 738877 (2021).
21. Almutairi, F. A. & Edrada-Ebel, R. A. Marine fungal metabolites: A promising source for antibiofilm compounds. *Molecules* **30**, 4266 (2025).
22. Rasconi, S., Jobard, M., Jouve, L. & Sime-Ngando, T. Use of calcofluor white for detection, identification, and quantification of phytoplanktonic fungal parasites. *Appl. Environ. Microbiol.* **75**, 2545–2553 (2009).
23. Lejars, M., Margaillan, A. & Bressy, C. Fouling release coatings: A nontoxic alternative to biocidal antifouling coatings. *Chem. Rev.* **112**, 4347–4390 (2012).
24. Brady, R. F. & Singer, I. L. Mechanical factors favoring release from fouling release coatings. *Biofouling* **15**, 73–81 (2000).
25. Kavanagh, C. J., Quinn, R. D. & Swain, G. W. Observations of barnacle detachment from silicones using High-Speed video. *J. Adhes.* **81**, 843–868 (2005).
26. Holland, R. et al. Adhesion and motility of fouling diatoms on a silicone elastomer. *Biofouling* **20**, 323–329 (2004).
27. Mori, K., Naito, M., Nakai, T., Fujiki, M. & Kawabe, T. Novel approach for biofouling-release materials with interpenetrating polymer networks. *MRS Online Proc. Libr. (OPL)* **897**, 0897-J03-02 (2005).
28. Thapliyal, P. C. Interpenetrating polymer networks. *Compos. Interfaces.* **17**, 85–89 (2010).
29. Tiwari, I. & Mahanwar, P. A. Polyacrylate/silica hybrid materials: A step towards multifunctional properties. *J. Dispers. Sci. Technol.* **40**, 925–957 (2019).
30. Allen, M. J. et al. Multimorphic materials: spatially tailoring mechanical properties via selective initiation of interpenetrating polymer networks. *Adv. Mater.* **35**, 2210208 (2023).
31. Yang, W. et al. The effect of wetting property on anti-fouling/foul-release performance under quasi-static/hydrodynamic conditions. *Prog. Org. Coat.* **95**, 64–71 (2016).
32. Wu, S. et al. Research progress of marine anti-fouling coatings. *Coat. 2024.* **14**, 1227 (2024).
33. Zhang, Z. et al. Fluorocarbon-based self-layering interpenetrating polymer-network coatings with anti-fouling and anti-icing properties. *Chem. Eng. J.* **474**, 145540 (2023).
34. Briand, J. F. et al. Spatio-temporal variations of marine biofilm communities colonizing artificial substrata including antifouling coatings in contrasted French coastal environments. *Microb. Ecol.* **74**, 585–598 (2017).
35. von Ammon, U. et al. The impact of artificial surfaces on marine bacterial and eukaryotic biofouling assemblages: A high-throughput sequencing analysis. *Mar. Environ. Res.* **133**, 57–66 (2018).
36. Briand, J. F. et al. Pioneer marine biofilms on artificial surfaces including antifouling coatings immersed in two contrasting French mediterranean Coast sites. *Biofouling* **28**, 453–463 (2012).
37. Papadatou, M. et al. Marine biofilms on different fouling control coating types reveal differences in microbial community composition and abundance. *Microbiologyopen* **10**, e1231 (2021).
38. Portas, A. et al. Impact of hydrodynamics on community structure and metabolic production of marine biofouling formed in a highly energetic estuary. *Mar. Environ. Res.* **192**, 106241 (2023).
39. Portas, A. et al. Shear stress controls prokaryotic and eukaryotic biofilm communities together with EPS and metabolomic expression in a semi-controlled coastal environment in the NW mediterranean sea. *Environ. Microbiome.* **19**, 1–16 (2024).
40. Catão, E. C. P. et al. Shear stress as a major driver of marine biofilm communities in the NW mediterranean sea. *Front. Microbiol.* **10**, (2019).
41. Song, F., Koo, H. & Ren, D. Effects of material properties on bacterial adhesion and biofilm formation. *J. Dent. Res.* **94**, 1027–1034 (2015).
42. Liu, Q. et al. Bacterial assembly during the initial adhesion phase in wastewater treatment biofilms. *Water Res.* **184**, 116147 (2020).
43. Gbaguidi, L. *Surfaces Antimicrobiennes Fonctionnelles écoresponsables* (Sorbonne Université, 2025).
44. Barret-Vivin V. Revêtements hybrides pour la protection de matériaux composites. (2016).
45. Medina, E. Synthèse de revêtements anticorrosion par voie sol-gel pour la protection de l'alliage 2024 T3. Caractérisation par spectroscopie d'impédance électrochimique et ellipsométrie in situ. (2019). https://theses.hal.science/tel-03053400/
46. Mieszkin, S., Martin-Tanchereau, P., Callow, M. E. & Callow, J. A. Effect of bacterial biofilms formed on fouling-release coatings from natural seawater and cobetia marina, on the adhesion of two marine algae. *Biofouling* **28**, 953–968 (2012).
47. Brzozowska, A. M. et al. Biomimicking micropatterned surfaces and their effect on marine biofouling. *Langmuir* **30**, 9165–9175 (2014).
48. Tan, J., Xu, J., Wang, D., Yang, J. & Zhou, S. Seawater-responsive SiO2 nanoparticles for in situ generation of zwitterionic polydimethylsiloxane antifouling coatings with underwater superoleophobicity. *J. Mater. Chem. Mater.* **8**, 24086–24097 (2020).
49. Candries, M., Atlar, M., Mesbahi, E. & Pazouki, K. The measurement of the drag characteristics of Tin-free Self-polishing Co-polymers and fouling release coatings using a rotor apparatus. *Biofouling* **19**, 27–36 (2003).

50. Matias, J. R. & Mary, A. Simulation of marine coating performance under natural tropical seawater conditions using the Poseidon Dynamic Test System.
51. Pau, G., Fuchs, F., Sklyar, O., Boutros, M. & Huber, W. EBImage—an R package for image processing with applications to cellular phenotypes. *Bioinformatics* **26**, 979–981 (2010).
52. Escadeillas, G., Bertron, A., Ringot, E., Blanc, P. J. & Dubosc, A. Accelerated testing of biological stain growth on external concrete walls. Part 2: quantification of growths. *Mater. Struct./Materiaux Et Constructions*. **42**, 937–945 (2009).
53. Oliveira, D. R. & Granhag, L. Ship hull in-water cleaning and its effects on fouling-control coatings. *Biofouling* **36**, 332–350 (2020).
54. Blanchet, E. et al. Quorum sensing and quorum quenching in the mediterranean seagrass posidonia oceanica microbiota. *Front. Mar. Sci.* **4**, 275926 (2017).
55. Romani, M. et al. High bacterial diversity in pioneer biofilms colonizing ceramic roof tiles. *Int. Biodeterior. Biodegrad*. **144**, 104745 (2019).
56. Lorenzen, C. J. Vertical distribution of chlorophyll and phaeo-pigments: Baja California. *Deep Sea Res. Oceanogr. Abstracts*. **14**, 735–745 (1967).
57. Martinez Ostormujof, L. et al. Systemic analysis of the Spatiotemporal changes in Multi-Species electroactive biofilms to clarify the gradual decline of current generation in microbial anodes. *ChemElectroChem* **10**, e202201135 (2023).
58. Buelow, E. et al. Hospital and urban wastewaters shape the matrix and active resistome of environmental biofilms. *Water Res.* **244**, 120408 (2023).
59. Hartmann, R. et al. Quantitative image analysis of microbial communities with BiofilmQ. *Nat. Microbiol.* **6**, 151–156 (2021).
60. Adouane, E., Hubas, C., Leblanc, C., Lami, R. & Prado, S. Multi-omics analysis of the correlation between surface microbiome and metabolome in Saccharina latissima (Laminariales, Phaeophyceae). *FEMS Microbiol. Ecol.* **101**, 160 (2025).
61. Epp, L. S. et al. New environmental metabarcodes for analysing soil DNA: potential for studying past and present ecosystems. *Mol. Ecol.* **21**, 1821–1833 (2012).
62. Fliegerova, K. et al. Effect of DNA extraction and sample preservation method on rumen bacterial population. *Anaerobe* **29**, 80–84 (2014).
63. Taberlet, P., Bonin, A., Zinger, L. & Coissac, E. Environmental DNA : for biodiversity research and monitoring. 253 (2018).
64. Bolyen, E. et al. Reproducible, interactive, scalable and extensible microbiome data science using QIIME 2. *Nat. Biotechnol.* **37**, 852–857 (2019).
65. Martin, M. Cutadapt removes adapter sequences from high-throughput sequencing reads. *EMBnet J.* **17**, 10–12 (2011).
66. Callahan, B. J. et al. DADA2: High-resolution sample inference from illumina amplicon data. *Nat. Methods*. **13**, 581–583 (2016).
67. Quast, C. et al. The SILVA ribosomal RNA gene database project: improved data processing and web-based tools. *Nucleic Acids Res.* **41**, D590–D596 (2013).
68. Nilsson, R. H. et al. The UNITE database for molecular identification of fungi: handling dark taxa and parallel taxonomic classifications. *Nucleic Acids Res.* **47**, D259–D264 (2019).
69. McMurdie, P. J. & Holmes, S. Phyloseq: an R package for reproducible interactive analysis and graphics of Microbiome census data. *PLoS One*. **8**, e61217 (2013).
70. Dixon, P. VEGAN, a package of R functions for community ecology. *J. Veg. Sci.* **14**, 927–930 (2003).
71. Rodrigues, A. M. S. et al. Straightforward N-Acyl homoserine lactone discovery and annotation by LC–MS/MS-based molecular networking. *J. Proteome Res.* **21**, 635–642 (2022).
72. Schmid, R. et al. Integrative analysis of multimodal mass spectrometry data in MZmine 3. *Nat. Biotechnol.* **41**, 447–449 (2023).
73. Wilkinson, L. ggplot2: elegant graphics for data analysis by WICKHAM. *H Biometrics*. **67**, 678–679 (2011).
74. Rohart, F., Gautier, B., Singh, A. & Lê Cao, K. A. MixOmics: an R package for 'omics feature selection and multiple data integration. *PLoS Comput. Biol.* **13**, e1005752 (2017).
75. Kolde, R. Package 'pheatmap'. (2025).
76. Nothias, L. F. et al. Feature-based molecular networking in the GNPS analysis environment. *Nat. Methods*. **17**, 905–908 (2020).
77. Dührkop, K. et al. SIRIUS 4: a rapid tool for turning tandem mass spectra into metabolite structure information. *Nat. Methods*. **16**, 299–302 (2019).
78. Dührkop, K., Shen, H., Meusel, M., Rousu, J. & Böcker, S. Searching molecular structure databases with tandem mass spectra using csi:fingerid. *Proc. Natl. Acad. Sci.* **112**, 12580–12585 (2015).
79. Dührkop, K. et al. Systematic classification of unknown metabolites using high-resolution fragmentation mass spectra. *Nat. Biotechnol.* **39**, 462–471 (2021).
80. Djoumbou Feunang, Y. et al. ClassyFire: automated chemical classification with a comprehensive, computable taxonomy. *J. Cheminform*. **8**, 1–20 (2016).
81. Kim, H. W. et al. NPClassifier: A deep neural network-based structural classification tool for natural products. *J. Nat. Prod.* **84**, 2795–2807 (2021).
82. Ludwig, M. et al. Database-independent molecular formula annotation using Gibbs sampling through ZODIAC. *Nat. Mach. Intell.* **2**, 629–641 (2020).
83. Shannon, P. et al. Cytoscape: A software environment for integrated models of biomolecular interaction networks. *Genome Res.* **13**, 2498–2504 (2003).
84. Baier, R. E. Surface behaviour of biomaterials: the theta surface for biocompatibility. *J. Mater. Sci. Mater. Med.* **17**, 1057–1062 (2006).
85. Caruso, G. Microbial colonization in marine environments: overview of current knowledge and emerging research topics. *J. Mar. Sci. Eng. 2020*. **8**, 78 (2020).
86. Bellou, N., Garcia, J. A. L., Colijn, F. & Herndl, G. J. Seasonality combined with the orientation of surfaces influences the microbial community structure of biofilms in the deep mediterranean sea. *Deep Sea Res. Part II*. **171**, 104703 (2020).
87. Georgiades, E., Scianni, C. & Tamburri, M. N. Biofilms associated with ship submerged surfaces: implications for ship biofouling management and the environment. *Front. Mar. Sci.* **10**, 1197366 (2023).
88. Chung, H. C. et al. Bacterial community succession and chemical profiles of subtidal biofilms in relation to larval settlement of the polychaete hydroides elegans. *ISME J.* **4**, 817–828 (2010).
89. Balducci, E., Papi, F. & Capialbi, D. E. Polysaccharides' structures and functions in biofilm architecture of Antimicrobial-Resistant (AMR) pathogens. *Int. J. Mol. Sci.* **24**, 4030 (2023).
90. Karygianni, L., Ren, Z., Koo, H. & Thurnheer, T. Biofilm matrixome: extracellular components in structured microbial communities. *Trends Microbiol.* **28**, 668–681 (2020).
91. Finnerty, S., Galán-Pérez, J. A., Li, Y., Kelleher, B. & O'Reilly, S. Molecular-level lipid studies on marine microphytobenthic biofilms: a mini-review. *Biochimie* https://doi.org/10.1016/J.BIOCHI.2025.09.004 (2025). doi:10.1016/J.BIOCHI.2025.09.004.
92. Panevska, A., Skočaj, M., Križaj, I., Maček, P. & Sepčić, K. Ceramide phosphoethanolamine, an enigmatic cellular membrane sphingolipid. *Biochim. Et Biophys. Acta (BBA) Biomembr.* **1861**, 1284–1292 (2019).
93. Borges, A. et al. Antibacterial activity and mode of action of selected glucosinolate hydrolysis products against bacterial pathogens. *J. Food Sci. Technol.* **52**, 4737 (2014).
94. Plaszkó, T., Szűcs, Z., Vasas, G. & Gonda, S. Effects of glucosinolate-derived isothiocyanates on fungi: A comprehensive review on direct effects, mechanisms, structure-activity relationship data and possible agricultural applications. *J. Fungi*. **7**, 539 (2021).

95. Patra, A. et al. Marine antimicrobial peptides-based strategies for tackling bacterial biofilm and biofouling challenges. *Molecules* **27**, 7546 (2022).
96. Qian, P. Y., Cheng, A., Wang, R. & Zhang, R. Marine biofilms: diversity, interactions and biofouling. *Nat. Rev. Microbiol.* **20**, 671–684 (2022).
97. Kettner, M. T., Rojas-Jimenez, K., Oberbeckmann, S., Labrenz, M. & Grossart, H. P. Microplastics alter composition of fungal communities in aquatic ecosystems. *Environ. Microbiol.* **19**, 4447–4459 (2017).
98. Kettner, M. T., Oberbeckmann, S., Labrenz, M. & Grossart, H. P. The eukaryotic life on microplastics in brackish ecosystems. *Front. Microbiol.* **10**, 415067 (2019).
99. Lacerda, A. L., d., F., Proietti, M. C., Secchi, E. R. & Taylor, J. D. Diverse groups of fungi are associated with plastics in the surface waters of the Western South Atlantic and the Antarctic Peninsula. *Mol. Ecol.* **29**, 1903–1918 (2020).
100. Oberbeckmann, S., Osborn, A. M. & Duhaime, M. B. Microbes on a bottle: Substrate, season and geography influence community composition of microbes colonizing marine plastic debris. *PLoS One*. **11**, e0159289 (2016).
101. Shearer, C. A. et al. Fungal biodiversity in aquatic habitats. *Biodivers. Conserv.* **16**, 49–67 (2007).
102. Jones, E. B. G. & Pang, K. L. Tropical aquatic fungi. *Biodivers. Conserv.* **21**, 2403–2423 (2012).
103. Banchi, E., Manna, V., Muggia, L. & Celussi, M. Marine fungal diversity and dynamics in the Gulf of Trieste (Northern Adriatic Sea). *Microb. Ecol.* **87**, 78 (2024).
104. Reich, M. & Labes, A. How to boost marine fungal research: A first step towards a multidisciplinary approach by combining molecular fungal ecology and natural products chemistry. *Mar. Genom.* **36**, 57–75 (2017).
105. Kauserud, H. ITS alchemy: on the use of ITS as a DNA marker in fungal ecology. *Fungal Ecol.* **65**, 101274 (2023).
106. Zhang, Z. F. et al. Culturing the uncultured marine fungi in the omics age: opportunities and challenges. *Fungal Biol. Rev.* **48**, 100353 (2024).
107. De Op, M., Persson, P. & Tunlid, A. Fungal extracellular polymeric substance matrices—Highly specialized microenvironments that allow fungi to control soil organic matter decomposition reactions. *Soil. Biol. Biochem.* **159**, 108304 (2021).
108. Breitenbach, R. et al. The role of extracellular polymeric substances of fungal biofilms in mineral attachment and weathering. *Npj Mater. Degrad.* **6**, 1–11 (2022).
109. Kjeldgaard, B. et al. Fungal hyphae colonization by Bacillus subtilis relies on biofilm matrix components. *Biofilm* **1**, 100007 (2019).
110. Gadd, G. M. Mycotransformation of organic and inorganic substrates. *Mycologist* **18**, 60–70 (2004).
111. Taboski, M. A. S., Rand, T. G. & Piórko, A. Lead and cadmium uptake in the marine fungi corollospora Lacera and *Monodictys pelagica*. *FEMS Microbiol. Ecol.* **53**, 445–453 (2005).
112. Vala, A. K. Tolerance and removal of arsenic by a facultative marine fungus *Aspergillus candidus*. *Bioresour Technol.* **101**, 2565–2567 (2010).
113. Pinto, A. P. et al. Degradation of terbuthylazine, Difenoconazole and pendimethalin pesticides by selected fungi cultures. *Sci. Total Environ.* **435–436**, 402–410 (2012).
114. Zhang, W. et al. A novel planar flow cell for studies of biofilm heterogeneity and flow-biofilm interactions. *Biotechnol. Bioeng.* **108**, 2571–2582 (2011).
115. Wang, S., Zhu, H., Zheng, G., Dong, F. & Liu, C. Dynamic changes in biofilm structures under dynamic flow conditions. *Appl. Environ. Microbiol.* **88**, (2022).
116. Zhang, L. et al. Preparation of superhydrophobic coating with anti-corrosion and anti-fouling properties on the surface of low manganese steel by electrodeposition. *Surf. Coat. Technol.* **460**, 129412 (2023).
117. Henry, B. J. et al. A critical review of the application of polymer of low concern and regulatory criteria to fluoropolymers. *Integr. Environ. Assess. Manag.* **14**, 316–334 (2018).

Acknowledgements

We acknowledge the Institut de l'Océan (Sorbonne Université) for founding Camille Ferré PhD grants and associated experiments. We acknowledge the Mutualized Aquariology Service (SMA) of the Oceanological Observatory of Banyuls-sur-Mer. We thank the teachers and students of Lycée Pablo Picasso (Perpignan, France) for their involvement in the conception and production of the laboratory rotor prototype, which was developed in the framework of an educational collaboration. We would also like to thank Alice Rodrigues for her assistance with the acquisition of MS/MS spectra and the Bio2Mar platform (http://bio2mar.obs-banyuls.fr) part of EMBRC France. We acknowledge the BioPic platform for its technical assistance. We are grateful to Argaly SA (Sainte-Hélène-du-LacSavoie, France; https://www.argaly.com) for performing the metabarcoding sequencing. We would like to thank Jérôme Charliac for his help with the formulation and characterization of the experimental coatings and Emeline Houël for helpful comments and editorial proofreading of the manuscript. Finally, we thank the reviewers for their constructive comments and their help to improve our manuscript.

Author contributions

C.F.: Conceptualization, methodology, project administration, formal analysis, data curation, investigation, visualization, writing – original draft, review and editing; L.G.: Conceptualization, methodology, formal analysis, writing – original draft, review and editing; S.F.: Data curation, investigation, validation, writing – original draft, review and editing; C.C.: Methodology, formal analysis, data curation; E.A.: Methodology, formal analysis, validation, writing-original draft, review and editing; Y.G.: Methodology, writing – review and editing; L.N.: Methodology, supervision, validation, writing – original draft, review and editing; and R.L.: Methodology, supervision, validation, writing – original draft, review and editing.

Funding

This research was funded by the Institut de l'Océan (Sorbonne Université).

Declarations

Competing interests

The authors declare no competing interests.

Additional information

Supplementary Information The online version contains supplementary material available at https://doi.org/1

0.1038/s41598-026-35567-6.

Correspondence and requests for materials should be addressed to R.L.